Multiscale mechanical characterization of mineral-reinforced wood cell walls

Steven A. Soini[1], Inam I. Lalani[2], Matthew L. Maron[2], David Gonzalez[3], Hassan Mahfuz[3], Neus Domingo[4], Vivian Merk[1*]

1 Florida Atlantic University, Department of Chemistry and Biochemistry, Department of Ocean and Mechanical Engineering, 777 Glades Rd, Boca Raton, FL-33431, USA

2 University of Miami, Department of Mechanical and Aerospace Engineering, 1251 Memorial Dr, Coral Gables, FL-33146

3 Florida Atlantic University, Department of Ocean and Mechanical Engineering, 777 Glades Rd, Boca Raton, FL-33431, USA

4, Center for Nanophase Materials Sciences, Oak Ridge National Laboratory, 1 Bethel Valley Road, Oak Ridge, TN-37830, USA

* Corresponding author

Abstract

Studying the multiscale mechanics of bio-based composites offers unique perspectives on underlying structure-property relations. Cellular materials, such as wood, are highly organized, hierarchical assemblies of load-bearing constituents that respond to mechanical stimuli at the microscopic, mesoscopic and macroscopic scale. In this study, we modified oak wood with nanocrystalline ferrihydrite, a widespread ferric oxyhydroxide mineral, and characterized the resulting mechanical properties of the composite at various levels of organization. Ferrihydrite nanoparticles were deposited inside the wood cell wall by an in-situ chemical reaction, resulting in increased stiffness and hardness of the functionalized secondary cell wall of fibers, as evidenced by region-specific nanoindentation tests under an electron microscope. Chemically modified and pristine wood samples were characterized using Atomic Force Microscopy in the bimodal frequency modulation mode, which produced topographical images from the cellular ultrastructure with high lateral resolution and localized nanomechanical information across distinct cell wall layers. The fracture behaviour of treated and reference wood at the macroscopic level was examined using bulk compression testing.

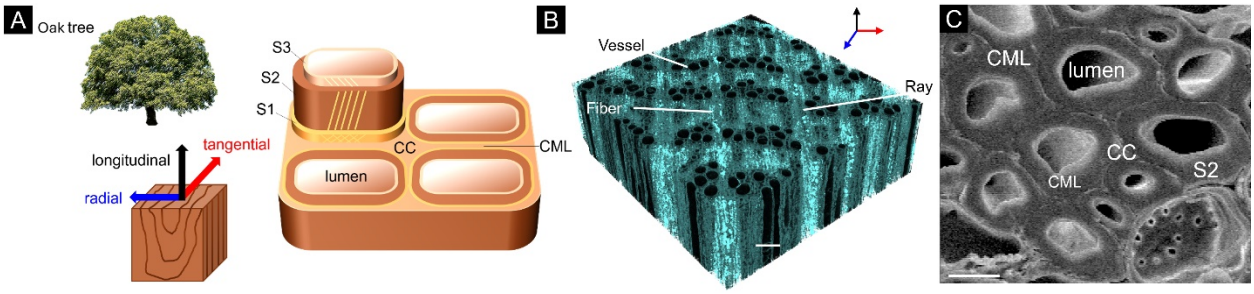

Figure 1. A) Schematic depicting oak tree, orthotropic directions of wood block and wood cell wall layer model. B) X-ray microtomography from Fh-mineralized oak wood. Turquoise-colored regions indicate X-ray absorbing Fh mineral. Scalebar equals 1 mm. C) Scanning Electron Micrograph from mineralized secondary cell walls. Scalebar correspond to 10 µm.

Introduction

The creation of functional materials from sustainable resources has become a significant area of focus within material science and engineering. Naturally occurring materials, such as lignocellulose, can be easily sourced from biomass, such as plant waste, and further modified to improve their macroscopic properties. Such chemical modification strategies offer new approaches for devising advanced high-performance materials, effective design concepts and structural optimization. One of the largest classes of renewable resources is wood, with approximately 181.5 billion tons being produced globally every year. Lignocellulose is a complex porous composite composed of three main biopolymers, cellulose, hemicellulose, and lignin, arranged in an anisotropic, hierarchical structure. At the macroscopic scale, wood is composed

of a honeycomb network of hollow cells joined by the compound middle lamella (CML). The high porosity of wood ensures remarkable mechanical stability at low specific density. Wood cell walls can be distinguished by their microfibril angle (MFA), which is defined as the tilt angle of the cellulose microfibrils that wind helically around the axial cell axis.[1] In the bulky secondary cell wall (S2), the cellulose microfibrils wind around the empty cell lumen at a steep 10-30° angle, providing mechanical rigidity under axial load.[1,2,3] In contrast, microfibrils in the adjacent S1 layer are arranged in a cross fibrillar structure oriented approximately perpendicular to the longitudinal axis, corresponding to a MFA of 70-90°.[1,2,3] The S3 layer bordering the lumen interface contains microfibrils that trace a flat helix (MFA > 60-90°) of opposite winding direction with respect to the S2 layer. Adjacent cells are joined by an adhesive layer rich in pectin and lignin, the compound middle lamella (CML) and the cell corners (CC).[1,2,3] Hardwoods tend to be denser and more durable than softwoods, making them suitable for furniture, flooring, and cabinetry. Hardwoods contain thick, short fibers that provide mechanical support and large, interconnected vessels that facilitate water conduction via perforation plates.[4] The present experimental study focused on ring-porous hardwood, which is sourced from broad-leaved, usually deciduous trees, such as oak, maple, cherry, and walnut. Ring-porous wood is characterized by a ring of large vessel elements, which transport water from the roots to the leaves.

In this study, environmentally benign iron (hydr)oxide was precipitated within North American Red Oak (*Quercus rubra*) using a straightforward *in situ* chemical reaction of ferric nitrate and potassium hydroxide.[5] The reaction yielded the poorly crystalline hydrous ferric oxyhydroxide mineral ferrihydrite (Fh). As natural part of soil and sediments, iron (hydr)oxides play a major role in the geochemical cycling of iron and metallurgical ore processing.[6] Being extraordinarily hard and stiff[7], iron (hydr)oxides have been blended into hybrid polymer composites to achieve mechanical reinforcement.[8,9,10] Similarly, limpet and chiton molluscs grow ultrahard teeth by mineralizing organic chitin scaffolds with the iron (hydr)oxides goethite, ferrihydrite, magnetite, or santabarbareite.[11,12,13] The ultra-low solubility of iron (hydr)oxides, such as Fh, ensures complete immobilization of the mineral phase in an organic matrix[14,15]. As previously shown by chemical Raman mappings, electron microscopy and X-ray microtomography, this functionalization protocol specifically targets the sub-microporous cell wall as opposed to the macroscopic void spaces of the cell lumen[5]. We found that nanocrystalline iron oxide is preferentially formed inside the secondary cell wall, along the compound middle lamella and in radial parenchyma cells[5].

In the present work, we address the question whether ultrahard minerals can be used to improve the mechanical properties of the cell wall through nanoscale confinement while maintaining a low specific density, small ecological footprint, and cost effectiveness. So far, only relatively few studies have systematically investigated the mechanical behaviour of chemically[16,17,18,19] or thermally[20,21,22] treated wood materials across multiple length scales. Given the complex architecture of biological materials, bridging various orders of hierarchy is the key to exploring the mechanisms of load bearing and failure in hybrid bio-based composites. To test our hypothesis that the insertion of nanocrystalline inorganic minerals into cell walls results in cell-wall-specific mechanical reinforcement, we applied multiscale mechanical testing using bimodal amplitude modulation frequency modulation Atomic Force Microscopy (AM-FM), nanoindentation inside the scanning electron microscope (SEM) and conventional bulk compression testing. Region-specific mechanical testing allowed us to probe local mechanical properties on a miniature length scale and pinpoint the macroscopic deformation and fracture behaviour. In the Atomic Force Microscope, nanomechanical mappings can be generated by collecting individual force-distance curves or through parametric multichannel imaging methods, such as viscoelastic mapping with AM-FM, which operates two cantilever resonances simultaneously.[23,24,25] In the present study, we employed bimodal AM-FM imaging: by oscillating the AFM tip at multiple frequencies, in which the first resonance frequency of the cantilever is used for imaging in tapping mode and modulated to maintain a constant amplitude of oscillation, while a higher resonance mode is operated in frequency modulation (FM) to simultaneously measure the elastic (storage) and viscous (loss)

properties of materials at the nanoscale.[26] Using AM-FM AFM, we gained detailed knowledge on changes in sub-cell wall level mechanics post treatment. In addition to these region-specific mechanical characterization methods, bulk mechanical testing provided stress-strain curves and fracture patterns of large unembedded wood samples under axial and radial load.

Materials and Methods

Materials

American Red Oak wood (*Quercus rubra*) was purchased from The Home Depot and cut using a band saw. Ferric nitrate nonahydrate (98%+, $Fe(NO_3)_3 \cdot 9H_2O$) and potassium hydroxide (KOH) were purchased from Alfa Aesar and used without further purification. Araldite GY 502, dodecenyl succinic anhydride (DDSA), and 2,4,6-tris-(dimethylaminomethyl)phenol (96%+, DMP-30) were acquired from Electron Microscopy Sciences.

Mineralization

To limit variations in the MFA, density, or other confounding factors, sequential wood blocks were cut from the same wood slab oriented in the longitudinal direction. In doing so, we minimized inherent variations in density, number and direction of growth rings, allowing us to directly compare treated and native samples. For micro- and nanomechanical testing, 5mm x 5mm x 5mm oak wood cubes were cut to size and immersed in a 0.2M solution of $Fe(NO_3)_3 \cdot 9H_2O$ in Milli-Q® ultrapure water (resistivity 18.2MΩ·cm at 25° C) for 24h using alternating vacuum-impregnation. Subsequently, an aqueous 1.0M KOH solution was added dropwise under constant stirring until the solution reached a pH of 7-8 before applying vacuum impregnation again. After 24h, samples were thoroughly washed with deionized water to remove any loose surficial mineral phase and air dried for at least 24 hours. For bulk mechanical testing, 25mm x 20mm x 20mm (L x R x T) samples were modified as described above and washed for a week to remove residual salts. After drying, the samples were weighed and measured to determine mass gain and any dimensional changes resulting from the treatment. A weight gain of 0.9354% was determined from a total of 20 sample measurements.

Scanning Electron Microscopy

Scanning electron microscopy (SEM) was carried out on a Coxem EM-30N instrument driven by an accelerating voltage of 15 kV in high-vacuum mode. Prior to SEM imaging, microtome-planed block faces were mounted onto Al stubs using carbon tape and sputter-coated with a thin layer of Pt under an argon atmosphere at 8 mA for 30 s using a MicroNanoTools MNT-JS1600 plasma sputtering coater.

X-ray microtomography

X-ray micro-computed tomographies were collected from mineralized oak samples using a Bruker Skyscan 1173 X-ray microCT scanner utilizing a voltage of 60 kV, current of 133 mA, pixel size of 7.917mm and rotation between sequential captured images of 0.16°.

Dehydration, Resin Embedding and Ultramicrotome Sectioning

After air drying, samples were dehydrated using an ethanol series (EtOH/H2O: 25/75, 50/50, 75/25, 90/10, 100/0, 100/0) and transferred to a solution of 100% propylene oxide in preparation for resin embedding. An epoxy resin mixture of 11 mL araldite and 10 mL DDSA was made, and samples were immersed in a series of resin/propylene oxide solutions (Resin/Prop Ox: 33/66, 66/33, 100/0, 100/0) before being placed in 100% resin mixture containing DMP-30 as the polymerizing agent. Samples were transferred into an oven and cured at 60˚C for at least 24h. Resin blocks were cooled and planed using a Leica Ultracut EM UC7RT ultramicrotome equipped with a Diatome 35° diamond knife to a final cutting increment of 50 nm. 2 mm tall samples were

cut from planed resin blocks using a Buehler Isomet 1000 diamond precision saw and mounted on 15 mm aluminum stubs with the ultramicrotomed surface facing up.

Tandem Nanoindentation – SEM imaging

Hardness and rigidity values of resin-embedded samples were measured with a Bruker PI 88 Pico indenter and triangular shaped Berkovich tip. A quartz reference sample was used to calibrate the instrument prior to all measurements. The nanoindenter was mounted inside a Zeiss UltraPlus field-emission scanning electron microscope (FE-SEM) to collect high-resolution images from the cell wall ultrastructure and position the indenter on the S2 cell wall of fiber cells. Indentation curves were obtained under displacement control with a loading rate of 4 nm/s to a maximum depth of 300nm followed by a 10 second hold and unloading rate of 4 nm/s until the force on the tip reached 0N. Data was analyzed with the Bruker Triboscan software to obtain values for hardness and reduced elastic modulus of each loading and unloading curve. Five indentations were collected for both the treated and untreated samples and averaged to obtain the elastic modulus and hardness values of pristine and treated wood. The reduced elastic modulus (Er) and hardness (H) were calculated according to the method of Oliver and Pharr[27].

Bimodal amplitude-frequency-modulation Atomic Force Microscopy (AM-FM)

Viscoelastic measurements of samples were acquired using bimodal amplitude-frequency-modulation (AM-FM) Atomic Force Microscopy using a Cypher AFM platform (Asylum Research-an Oxford Instruments company). AM-FM images were processed using Igor Pro 6.3 and AR 16.10.211 to obtain the Young's modulus and indentation depth of the AFM probe.

Bulk compression testing

Compressive tests bulk mechanical tests were performed with a Zwick-Roell Z050 materials testing machine under displacement control at 20°C and 65% relative humidity. We tested modified and pristine oak wood in the longitudinal and radial direction, using at least 10 replicates per permutation. Measurements were then converted to stress and strain values using the cross-sectional area of each sample.

Results and Discussion

The distribution of the ferrihydrite mineral phase within hardwood has been described in previous works by the authors[5]. The ferrihydrite mineral phase was shown to infiltrate all cell wall layers, suggesting a substantial impact on the micro- and nanoscale mechanical properties of the structure. The inclusion of a significant weight percentage (15-20%) of Fh and its homogenous distribution throughout the material were therefore expected to result in mechanical reinforcement. The current study quantifies mechanical properties of chemically altered wood cell walls at the bulk, micro-, and nanoscale.

Nanoindentation/SEM

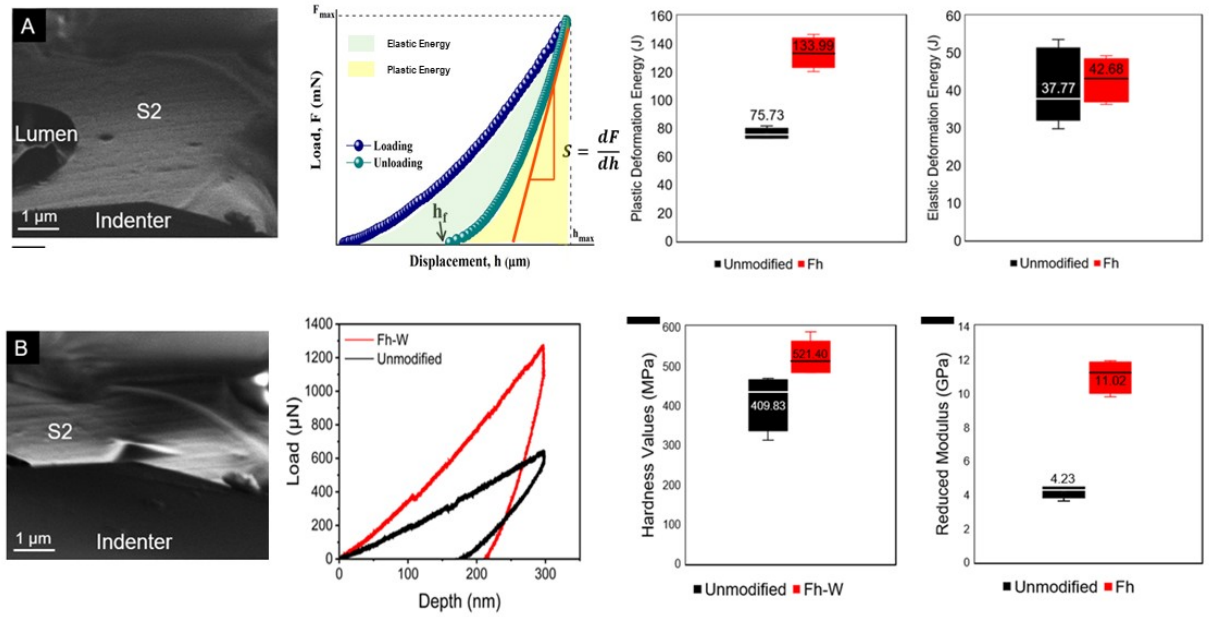

Figure 2. An overview of SEM-nanoindentation with A) indenter alignment over region of interest and B) indentation of S2 cell wall. XX Comparison of hardness and reduced modulus (E_R) values for unmodified (black) and Fh-treated (red) oak wood, respectively.

To study cell-wall-specific reinforcement, we simultaneously imaged the deformation and failure behavior of modified wood using an electron microscope. Load-displacement curves revealed the deformation mechanisms of the cell walls when indented. Nanoindentation within an SEM is beneficial, as it allowed us to accurately place the nanoindenter with micron-precision at the half width of the S2 cell wall of hardwood fibers, thereby minimizing errors arising from the proximity of other cell wall layers or the resin-penetrated lumen. Resin infiltration of wood materials has previously been found to increase apparent hardness measured by nanoindentation[28,29,30], while other factors, such as cutting direction during specimen preparation, and Berkovich tip geometry did not prove relevant for nanoindentation results[31]. In the present study, treated and untreated samples were prepared using identical resin batches to minimize variations from the embedding agent. Reference measurements from the embedding medium within the lumina were taken to account for possible influence on mechanical properties. However, we confirmed that the stiffness of the embedding medium relative to the sample was insignificant in terms of scale. Smooth sample surfaces were created by ultramicrotoming with a diamond knife. Based on indentation loading-unloading curves as shown in Figure XX, it is possible to obtain the elastic and plastic energies for the deformation as the areas below the load and unload curves respectively, and also calculate the reduced Young modulus and hardness as describe in the supplementary material. By using equation SX and tabulated Poisson's ratios of oak (μ_{LR}= 0.35 at 12% moisture content), the reduced modulus values E_R obtained by fitting the load-depth curves were converted to Young's Modulus values of 3.75 GPa and 9.67 GPa for the Fh-treated and reference samples, respectively.

The obtained reduced Young Modulus were found to be substantially higher in the Fh-containing samples than in the references. The hardness of reference wood cell walls , as obtained from equation SY, was in excellent agreement with literature values obtained by contact-resonance AFM[19] or nanoindentation with a Berkowich tip[31]. Upon chemical modification, the values for the

reduced modulus and hardness were found to increase by 260.5% and 127%, respectively (Figure 2X,2Y). Remarkably, the relative improvement of reduced modulus and hardness from the mineralization with nanocrystalline Fh exceeded the ones observed in phenol formaldehyde glue infiltrated wood.[19,29] It is known that the modulus of elasticity is negatively correlated with the MFA, which corresponds to higher stiffness along the fiber direction, while there is only a weak correlation between hardness and MFA[31]. Hardness, however, is closely connected to the chemical composition of the cell wall matrix.[31]

We further quantified the elastic and plastic energy dissipation during the impact of the indenter on the wood surface. Elastic deformation energy is fully dissipated through heat, whereas plastic energy is defined as energy dissipated by plastic deformation of the sample. Based on our results, the elastic deformation energy remained almost constant (Figure 2Z), while the plastic deformation energy almost doubled after chemical modification (Figure 2W), which can contribute to the damage tolerance of the composite. However, there are several practical limitations with regards to nanoindentation of wood, the main being a relatively small sample size and the destructive nature of measurement collection[32]. Previous nanoindentation studies of wood have found substantial differences between latewood and earlywood, and even within the same domain of an individual cell wall, making a larger number of indentations imparative to accurately determining the mechanical information of the cell wall.[32]

Functional Atomic Force Microscopy

Using functional Atomic Force Microscopy, thousands of nanomechanical data points can be quickly collected in a nondestructive manner, allowing for reproducible measurements to be performed. In this study, elastic and viscoelastic properties of chemically modified and pristine wood were probed using the bimodal AM-FM technique to evaluate the sample stiffness, degree of tip indentation, and energy dissipation, which serves as a measure of sample hardness (Figure 3-5). This methodology, while not revealing exact mechanical information, allows for comparative studies between samples and regions of interest. In this way, large sections of entire cells can be measured with nanoscale resolution in contrast to individual indentations averaging the load over several hundreds of nanometers (or even microns), allowing for the collection of thousands of data points from large areas. This huge dataset allows for a more comprehensive mechanical characterization of distinct cell wall layers. Color-coded AM-FM measurements allowed us to characterize oak cross sections based on differences in cellular morphology, energy dissipation and Young's Moduli. The histograms in Figure 4G give the Gaussian distribution of Young's Moduli over lumen-free cell wall regions. Based on AM-FM results, the average Young's modulus of the composite increases by 314% when comparing to pristine oak wood (Figure 4G), which is in excellent agreement with the destructive nanoindentation measurements from S2 cell walls. Adhesion force differences can reveal chemicals variations within the biological tissue, for instance higher proportions of amorphous hemicellulose or lignin, resulting in hydrophilic or hydrophobic properties[33,34].

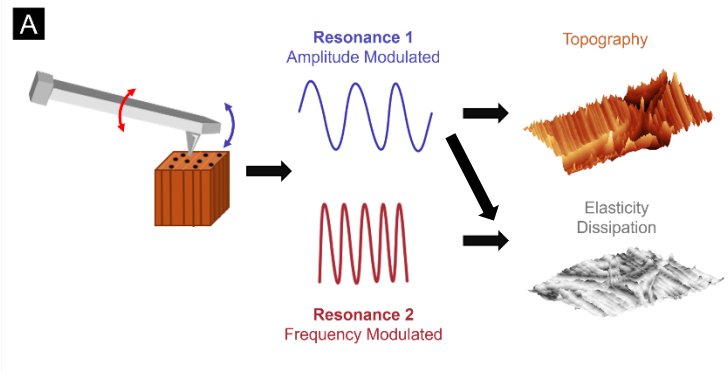

Figure 3. A) Diagram of AM-FM AFM set-up highlighting the two simultaneous resonance frequencies to derive topographical and mechanical sample information.

Interestingly, the histograms show a multimodal stiffness distribution in both Fh-treated and pristine wood, which reflects local variations in elastic moduli. Apart from the inherent variability of wood as biological material, such heterogeneity could be attributed to variations in cell wall thickness, the degree of lignification or the microfibril orientation within individual cell wall layers (not to mention a certain contribution of topographical cross-talk, observed as the stripes produced when cutting the sample). In addition, we found a wider spread of stiffness values in chemically modified than in native wood, which could hint towards a heterogeneous distribution of nanocrystalline Fh across the cell wall. However, when comparing AM-FM histograms from modified and reference samples, it is evident that these domains are reinforced by the same factor, supporting our finding that the cell wall has been strengthened across multiple layers, in contrast to solely the bulky S2 cell wall layer.

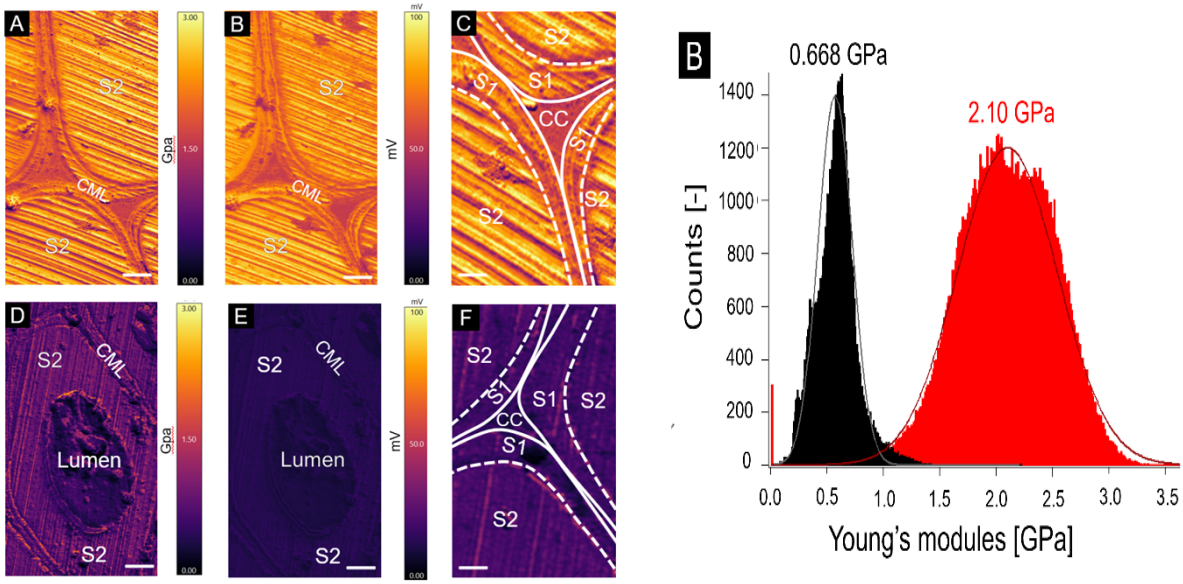

Figure 4. 10 µm^2 AM-FM mappings of Fh treated (A-C) and unmodified oak wood (D-F). A,D) Young's modulus and B,E) energy dissipation. C,F) Distinction of cell wall layers in zoom-in image of (young modulus or energy dissipation??). The diagonal lines are knife marks resulting from imperfections of the diamond knife. Scalebars corresponds to 1 µm. G) Histograms showing mulimodal distribution of Young's moduli in pristine and chemically modified *Quercus rubra*.

Color-coded AFM images visualize the distribution in elastic modulus and viscoelastic response, such as local energy dissipation, of different cell wall regions (Figure 5). We calculated the Young's moduli from ~1 x 1 μm^2 regions of interest to verify whether the three stiffness maxima displayed in Figure 4 stem from cell wall regions that differ in their mechanical characteristics, such as the CML, S1 and S2 region, as previously observed in QI™ mode AFM imaging of unembedded spruce.[35] While the S2 layer makes up approximately 80% of the cell wall, the S1 and S3 cell wall layers play an important role in the mechanical behavior of the entire cell wall, whereas the CML is pivotal for cell-cell adhesion. The lower stiffness of the S1 and S3 layers is attributed to their larger MFA of 70-90°.[36] In the corresponding stiffness images and histograms,

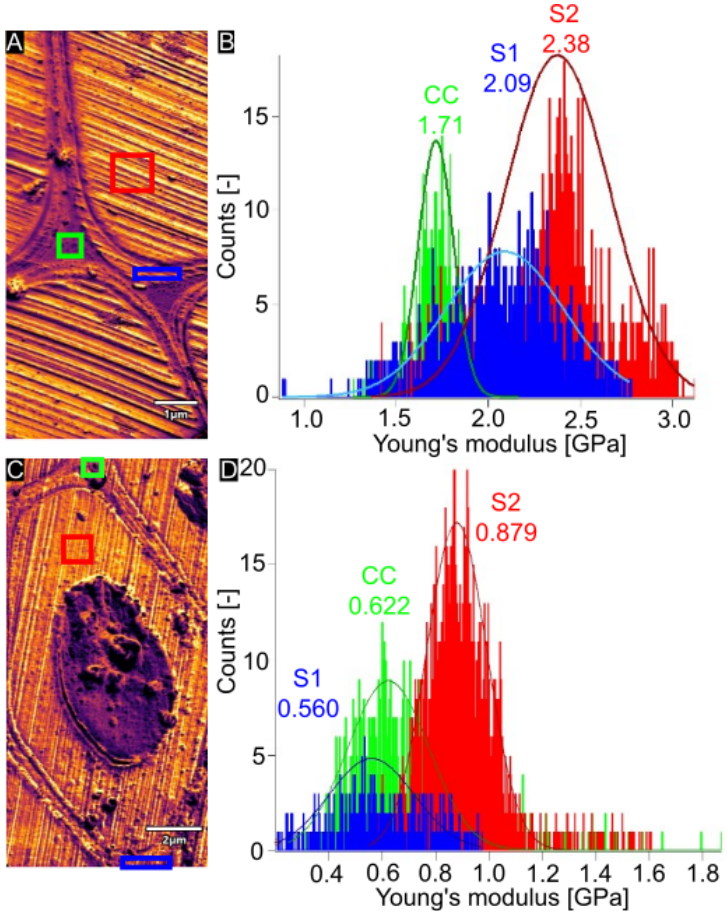

Figure 5. Histograms summarizing the Young's Moduli of the distinct cell wall layers from regions of interest in the cell corner (CC), S1 and S2 cell wall layers. Scalebars equal 2µm. A, B) Pristine wook and C,D) Fh-treated wood.

we can discern a narrower Gaussian distribution of Young's Modulus values in pristine wood than in Fh-treated wood, with a notable increase in mean values from 0.879 GPa to 2.38 GPa in the bulky secondary cell wall (Figure 6). Previous functional AFM measurement by Arnould *et al.*[37] and Casdorff et al.[35] found roughly two-times higher Young's Modulus values in the S2 layer compared to the CC or CML region. While we observed a similar trend in pristine oak, mechanical differences between CC and S2 in ferrihydrite-functionalized samples were far less drastic.

Bulk Compression Testing

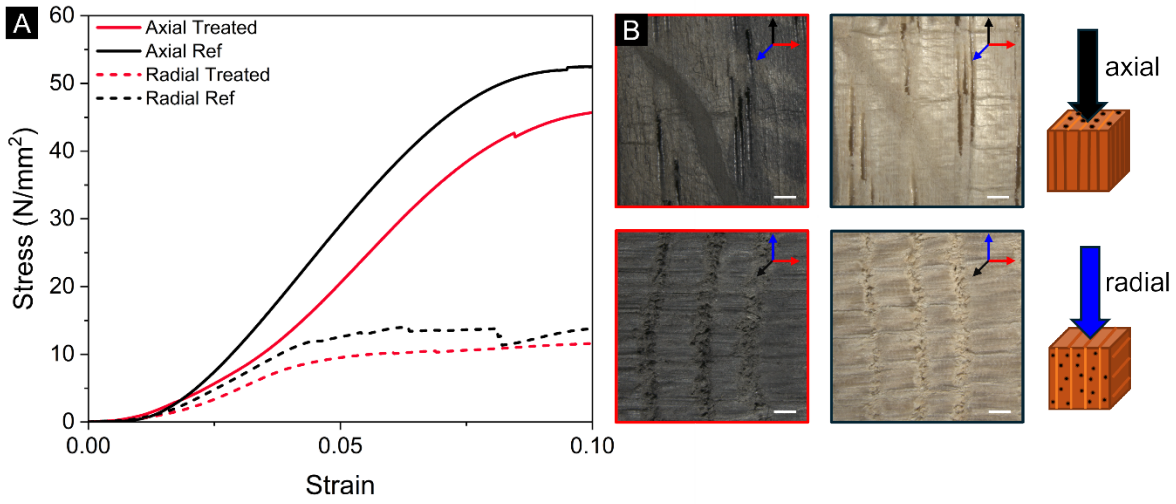

Figure 6. A) Typical stress/strain curves obtained from bulk compression studies in the axial (solid line) and radial direction (dashed line) of Fh-treated (red) and unmodified (black) samples. B) Images of treated (left) and untreated (right) wood samples post compression tests in the axial (top) and radial (bottom) directions showing similar deformation and fracture patterns. Scale bars correspond to 1 mm.

To assess bulk mechanical properties, mineralized and pristine wood samples were subjected to static compression tests to determine the modulus of elasticity, yield strength and maximum strength. In previous studies, the compressive strength of American Red Oak was measured to be 47.0-48.9 MPa and 8.6 MPa parallel and perpendicular to the grain under equilibrium moisture conditions.[38] Previous studies found a Young's modulus of 7.83 GPa in oak under compressive load[39], which is in good agreement with the present study. Herein, the compressive stiffness and strength of Fh-modified wood loaded in the axial direction were on average 26.23% lower than in the references. The apparent discrepancy between bulk and region-specific mechanical testing could have multiple explanations: One reason could be that the crystalline order of the cellulose microfibers was disrupted under harsh acidic reaction conditions. Even though the pH was maintained at a near-neutral pH value of 7-8 to induce mineral precipitation, samples were exposed to a highly acidic (pH < 1) precursor solution of ferric nitrate for an extended amount of time to allow for homogeneous mineralization across large sample volumes. It is possible that such extreme pH conditions degrade or leach wood polymers by acidic hydrolysis[32], which could impair the mechanical integrity of the cell wall. In addition, an increased amount of amorphous cellulose could be associated with a higher relative moisture content. Residual hygroscopic salts (e.g., KOH, KNO_3) could further increase the relative equilibrium moisture content, which is known to negatively affect the mechanical performance of wood.[40,41,42] It is noteworthy that we observed more comparable stiffness and strength in modified and control samples when samples were compressed in the radial direction across the grain. This could be due to the preferential deposition of Fh mineral in rays, compensating for comparably lower strength in the axial direction. We further elucidated potential changes in the failure mechanism of chemically altered wood. Despite the lower stiffness and compressive strength in Fh-containing wood, bulk mechanical testing did not reveal pronounced differences in the deformation and fracture patterns of treated and native oak wood. The two most important fracture paths in wood are cell fracture and cell separation.[43,44] Similar to previous studies on compressive testing of oak[39], we observed multiple failure patterns, including pear-shaping, shearing, wedge-splitting and splitting (rupture parallel to the grain). Previous studies showed that radial cracks follow a tortuous path, primarily propagating through alternating layers of early- and latewood in a stick-slip manner.[45] The presence of residual iron salts is expected to weaken cell-cell adhesion along the compound

middle lamella, resulting in delamination along the CML, while leaving the secondary cell wall intact.[45]

A limitation of the present study is that region-specific mechanical testing focused on the cross section of thick-walled fibers, which primarily provide mechanical support in the living tree. We did not elucidate the cell wall mechanics in other anatomic regions, e.g., water-conducting vessels, pits, or parenchyma cells in rays, that are an integral part of the micro- and mesostructure of hardwood. Vessels, for instance, can potentially influence crack propagation through crack-tip blunting or crack deflection.[43] Discrepancies between AM-FM AFM and nanoindentation results, as observed by other authors, can be caused by differences in geometry between nanoindenter probe and AFM tip and their indentation depth[37,46,34]. In the present study, substantially lower Young's modulus values were measured in AFM compared to nanoindentation, which can be explained by the smaller interaction volume of the probe during indentation[37,46,34]. Another factor could be the inclination of the faces of the Berkovich-type indenter, which changes the loading angle of the cell wall[47]. Cross-study comparisons of AFM data from wood materials are often complicated by differences in sample preparation protocols, wood species, cell type, assumed mechanical model, hydration state, surface and imaging artefacts[48]. Another factor is that the mechanical properties of solid wood are closely related to the material's density. While it is generally assumed that plant cell walls have a constant bulk density of 1500 kg/m^3 independent of the wood species[32], the chemical modification is likely to increase the cell wall density due to the incorporation of nanocrystalline iron hydroxide.

Conclusions

Taken together, this research enhances our understanding of structure-function relationships in hierarchical biological materials, particularly the mechanical response of fibrous multi-component systems. Using a straightforward and cost-effective chemical modification approach based on benign nanocrystalline iron oxyhydroxide, we achieved mechanical reinforcement of the cell wall at minimally increased density. By analyzing complex composite materials such as solid wood at different levels of organization, we gleaned new information on how to engineer and chemically alter biological materials for practical applications. Functional AFM, such as bimodal amplitude-modulated and frequency-modulated AFM, proved useful for inferring detailed ultrastructural and mechanical information of chemically functionalized wood. Bio-based composites bear the potential of replacing conventional engineering materials such as steel or concrete in the construction of multistory buildings, bridges, furniture and flooring.

Acknowledgements

SS acknowledges support by a Department of Energy (DOE) Office of Science Graduate Student Research (SCGSR) fellowship. VM thanks the National Science Foundation (NSF2137663, Division of Materials Research) for partial financial support. We thank Dr. Giacomo Po, Assistant Professor at the University of Miami, for providing access to combined nanoindentation/SEM experiments. Advanced AFM studies were conducted as part of the user project CNMS2023-B-02186 at the Center for Nanophase Materials Sciences (CNMS), which is a US Department of Energy, Office of Science User Facility at Oak Ridge National Laboratory. We thank the Owls Imaging Lab at FAU High School (FAUHS) for providing access to a X-ray microCT scanner. Research technician Jamie Knaub is acknowledged for technical support during X-ray microtomography scans.

References

1 J. Fahlén and L. Salmén, *Plant Biol.*, 2002, **4**, 339–345.

2 D. Fengel and G. Wegener, *Wood – Chemistry, Ultrastructure, Reactions*, de Gruyter, New York, 1989.

3 N. Hon, David; Shiraishi, *Wood and Cellulosic Chemistry*, CRC Press, Boca Raton, 2nd edn., 2000.

4 H. Xu, A. Giannetti, Y. Sugiyama, W. Zheng, R. Schneider, Y. Watanabe, Y. Oda and S. Persson, *Open Biol.*, 2022, **12**, 210208.

5 S. A. Soini, S. M. Feliciano, B. G. Duersch and V. M. Merk, *RSC Sustain.*, 2024, **2**, 626–634.

6 J. L. Jambor and J. E. Dutrizac, *Chem. Rev.*, 1998, **98**, 2549–2586.

7 J. R. Nicholls, D. J. Hall and P. F. Tortorelli, *Mater. High Temp.*, 1994, **12**, 141–150.

8 H. S. Mahmood and N. F. Habubi, *Appl. Phys. A*, 2022, **128**, 956.

9 S. Varghese, J. P. Chaudhary and C. Ghoroi, *RSC Adv.*, 2020, **10**, 13394–13404.

10 W. Ojok, E. Ntambi, J. Bolender, J. Wasswa, W. Wanasolo and B. Moodley, *Carbohydr. Polym. Technol. Appl.*, 2022, **4**, 100241.

11 R. M. H. Rumney, S. C. Robson, A. P. Kao, E. Barbu, L. Bozycki, J. R. Smith, S. M. Cragg, F. Couceiro, R. Parwani, G. Tozzi, M. Stuer, A. H. Barber, A. T. Ford and D. C. Górecki, *Nat. Commun.*, 2022, **13**, 3753.

12 J. C. Weaver, Q. Wang, A. Miserez, A. Tantuccio, R. Stromberg, K. N. Bozhilov, P. Maxwell, R. Nay, S. T. Heier and E. DiMasi, *Mater. Today*, 2010, **13**, 42–52.

13 L. Stegbauer, P. J. M. Smeets, R. Free, S. G. Wallace, M. C. Hersam, E. E. Alp and D. Joester, *Proc. Natl. Acad. Sci.*, 2021, **118**, e2020160118.

14 R. M. Schwertmann, Udo; Cornell, *Iron Oxides in the Laboratory*, Wiley-VCH, Weinheim; Chichester, 2 edition., 2000.

15 R. M. Cornell and U. Schwertmann, *The iron oxides: structure, properties, reactions, occurrences and uses*, John Wiley & Sons, 2003.

16 C. Gusenbauer, D. S. Jakob, X. G. Xu, D. V Vezenov, É. Cabane and J. Konnerth, *Biomacromolecules*, 2020, **21**, 4244–4252.

17 L. S. Martin, S. Jelavić, S. M. Cragg and L. G. Thygesen, *Green Chem.*, 2021, **23**, 8003–8015.

18 M. Frey, D. Widner, J. S. Segmehl, K. Casdorff, T. Keplinger and I. Burgert, *ACS Appl. Mater. Interfaces*, 2018, **10**, 5030–5037.

19 X. Wang, Y. Deng, Y. Li, K. Kjoller, A. Roy and S. Wang, *RSC Adv.*, 2016, **6**, 76318–76324.

20 X. Wang, Y. Deng, S. Wang, C. Min, Y. Meng, T. Pham and Y. Ying, 2014, **68**, 167–173.

21 G. A. Zickler, T. Schöberl and O. Paris, *Philos. Mag.*, 2006, **86**, 1373–1386.

22 E. Yurttas and N. Ayrilmis, *Macromol. Mater. Eng.*, 2023, **308**, 2300180.

23 R. Garcia, *Chem. Soc. Rev.*, 2020, **49**, 5850–5884.

24 S. Jesse, R. K. Vasudevan, L. Collins, E. Strelcov, M. B. Okatan, A. Belianinov, A. P. Baddorf, R. Proksch and S. V Kalinin, *Annu. Rev. Phys. Chem.*, 2014, **65**, 519–536.

25 D. Ebeling and S. D. Solares, *Beilstein J. Nanotechnol.*, 2013, **4**, 198–207.

26 C. Dietz, M. Schulze, A. Voss, C. Riesch and R. W. Stark, *Nanoscale*, 2015, **7**, 1849–1856.

27 S. V Kontomaris and A. Malamou, *Mater. Res. Express*, 2020, **7**, 33001.

28 R. Coste, M. Soliman, N. B. Bercu, S. Potiron, K. Lasri, V. Aguié-Béghin, L. Tetard, B. Chabbert and M. Molinari, *Compos. Sci. Technol.*, 2021, **201**, 108485.

29 Z. Li, K. Long, Y. Zhang, K. Chen and L. Lin, *Holzforschung*, 2022, **76**, 556–566.

30 L. Qin, L. Lin and F. Fu, *BioResources*, 2016, **11**, 182–194.

31 J. Konnerth, N. Gierlinger, J. Keckes and W. Gindl, *J. Mater. Sci.*, 2009, **44**, 4399–4406.

32 J. E. Jakes and D. S. Stone, *Forests*, 2021, 12.

33 C. Gusenbauer, E. Cabane, N. Gierlinger, J. Colson and J. Konnerth, *Sci. Rep.*, 2019, **9**, 18569.

34 A. C. Normand, A. M. Charrier, O. Arnould and A. L. Lereu, *Sci. Rep.*, 2021, **11**, 5739.

35 K. Casdorff, T. Keplinger and I. Burgert, *Plant Methods*, 2017, **13**, 60.

36 J. Brändström, S. L. Bardage, G. Daniel and T. Nilsson, *IAWA J.*, 2003, **24**, 27–40.

37 O. Arnould, D. Siniscalco, A. Bourmaud, A. Le Duigou and C. Baley, *Ind. Crops Prod.*, 2017, **97**, 224–228.

38 M. M. P. Data, American Red Oak Wood, https://www.matweb.com/search/DataSheet.aspx?MatGUID=f1530de2e5124fe997a436260d11a260.

39 J. Jiang, J. Lu, Y. Zhou, Y. Zhao and L. Zhao, *BioResources*, 2014, **9**, 3571–3579.

40 Y. Xie, Q. Fu, Q. Wang, Z. Xiao and H. Militz, *Eur. J. Wood Wood Prod*, 2013, **71**, 401–416.

41 Z. Cai and R. J. Ross, *Wood handbook-Wood as an Eng. Mater. Centen. Ed. Gen. Tech. Rep. FPL-GTR-190. Dep. Agric. For. Serv. For. Prod. Lab. Madison, Wisconsin, EUA*.

42 Y. Ishimaru, K. Arai, M. Mizutani, K. Oshima and I. Iida, *J. Wood Sci.*, 2001, **47**, 185–191.

43 M. P. C. Conrad, G. Smith and G. Fernlund, *Wood Fiber Sci.*, 2003, **35**, 570–584.

44 R. A. Luimes, A. S. J. Suiker, C. V Verhoosel, A. J. M. Jorissen and H. L. Schellen, *Wood Sci. Technol.*, 2018, **52**, 1243–1269.

45 F. Thuvander and L. A. Berglund, *J. Mater. Sci.*, 2000, **35**, 6277–6283.

46 K. Casdorff, T. Keplinger, M. Rüggeberg and I. Burgert, *Planta*, 2018, **247**, 1123–1132.

47 W. Gindl and T. Schöberl, *Compos. Part A Appl. Sci. Manuf.*, 2004, **35**, 1345–1349.

48 E. Toumpanaki, D. U. Shah and S. J. Eichhorn, *Adv. Mater.*, 2021, **33**, 2001613.